ELSEVIER

Ceramics International 30 (2004) 965–976

CERAMICS INTERNATIONAL

www.elsevier.com/locate/ceramint

Effect of raw-Si particle size on the properties of sintered reaction-bonded silicon nitride

Joo-Sin Lee [a,*], Ji-Hun Mun [a], Byung-Dong Han [b], Hai-Doo Kim [b], Byoung-Chul Shin [c], Il-Soo Kim [c]

[a] *Department of Materials Science and Engineering, Kyungsung University, Busan 608-736, South Korea*
[b] *Ceramic Materials Group, Korea Institute of Machinery and Materials, Changwon, Kyungnam 641-010, South Korea*
[c] *Department of Information Materials Engineering, Dongeui University, Busan 614-714, South Korea*

Received 4 August 2003; received in revised form 28 August 2003; accepted 5 November 2003

Available online 19 March 2004

Abstract

The effect of raw-Si particle size on the properties of sintered reaction-bonded silicon nitride (sintered RBSN) was investigated by the use of Si powders with different particle sizes containing various native SiO_2 oxide contents. Different secondary phases were formed in each specimen reaction-sintered with different particle sizes due to the content difference in native oxide on the surface layer of particles. The specimens prepared by using coarse powders did not show high density at high-temperature gas-pressure sintering, because of the abnormal growth of elongated β-Si_3N_4 grains owing to the insufficiency and the inhomogeneous distribution of the liquid phase. The specimens made with fine powders shows high density because of the melting of the secondary oxynitride phase. As a result, the content and distribution of the liquid phase became suitable for complete densification, which resulted in density increase. Higher values of fracture strength were obtained for the specimens made by using fine powders, however, higher values of fracture toughness were obtained when large elongated grains were developed in a fine grained matrix. The effects of sintering additives on the densification behavior of RBSN prepared by using coarse powders were also investigated. Densification near theoretical density was attained by using sintering additives, such as 6 wt.% Y_2O_3 + 3 wt.% Al_2O_3 + 2 wt.% SiO_2 (6Y3A2S) and 9 wt.% Y_2O_3 + 1.5 wt.% Al_2O_3 + 3 wt.% SiO_2 (9Y1.5A3S). In the case of 6Y3A2S addition, high fracture strength of 960 MPa and fracture toughness of 6.5 MPa $m^{1/2}$ were obtained.

Keywords: Sintered reaction-bonded silicon nitride; Oxynitride; Si particle size; Sintering additives

1. Introduction

Silicon nitride is one of the most promising ceramic materials for the use in gas turbine engines and other high-temperature structural applications because of its high-temperature strength, thermal shock resistance, chemical stability and excellent creep resistance [1].

There are various sintering methods to produce silicon nitride: hot-pressing, pressureless sintering and reaction-bonded sintering, etc. Among these, reaction-bonded silicon nitride (RBSN) offers a number of advantages over materials produced by more conventional processes, such as hot-pressing and pressureless sintering. In particular, complex shapes can be formed to meet precise dimensional tolerances with minimal or, in some cases, no machining. Also, RBSN produced by reaction bonding of silicon powder compacts is cheaper compared to sintered Si_3N_4, because the price of Si powder is much lower than that of Si_3N_4 powder. Reaction-bonding processes generally require lower fabrication temperatures than hot-pressing and pressureless sintering, which is a potential advantage for processing ceramic–matrix composites, where high temperatures can damage the reinforcement phase. However, the mechanical properties of RBSN sometimes cannot meet the high reliability and performance specifications required for advanced engineering applications due to the existence of pores in the reaction-bonded body. In order to make up for the demerits the postsintering process, where the reaction-bonded body is resintered at high temperatures with gas pressure, has been introduced [2,3].

* Corresponding author. Tel.: +82-51-620-4763; fax: +82-51-622-8452.
E-mail address: leejs@star.kyungsung.ac.kr (J.-S. Lee).

0272-8842/$30.00
doi:10.1016/j.ceramint.2003.11.003

In the reaction-bonding process the reaction mechanism is very complex, because the chemical reaction and sintering occur concurrently, and they depend on the process conditions, such as temperature, gas pressure, gas composition and heating schedule [4–9]. Also, the intrinsic factor, such as purity of raw materials, has an influence on the nitriding kinetics [10–12]. In particular, oxygen on the raw-Si powder surfaces has a strong influence not only on the nitridation but also on the gas-pressure sintering performed as a postsintering of the reaction-bonded body. It is not surprising that commercial Si powders typically have a native oxide (SiO_2) surface layer.

The existence of SiO_2 in producing silicon nitride ceramics can have an important role in the densification and phase equilibria by reacting with the sintering aids to form a liquid phase. The amount and composition of the liquid phase become important factors that control the microstructure and properties of the resulting Si_3N_4 ceramics.

Introduction of oxygen (SiO_2) in producing RBSN ceramics can occur due to several sources. It can be introduced by the native oxide on the raw-Si powder surfaces, the solvent [13], milling [14], the sintering atmosphere, and so on. Especially, since the oxygen (SiO_2) content of the starting Si powders can vary by a large difference depending on the particle size, it is expected to exert considerable influence on RBSN ceramics. The SiO_2 content increases by reducing the particle size of the raw-Si powders. It can also be expected that such a variation of SiO_2 content results in the appearance of various oxynitride crystalline phases during processing.

Only limited reports are available on the appearance of various silicon oxynitrides in RBSN ceramics. Kleebe and Ziegler [11] reported that various crystalline secondary phases were formed during nitridation of Si-powder compacts containing sintering aids. Their concentration depends on the chemical Si-powder characteristics and on the composition of additives. In their study, however, the range of variation in particle size or oxygen content was narrowly limited.

In this work, the effect of raw-Si particle size on the property of RBSN is studied by the use of Si powders with different particle sizes containing various native oxide SiO_2 contents. Emphasis is especially placed on the secondary phases formed during the nitridation process, the phase development with increasing temperature, the influence of secondary phases on the densification behavior and the microstructural development during postsintering, and the resulting mechanical properties of the sintered RBSN.

2. Experimental procedure

The Si powders (Permascand) used for this study consisted of three kinds: coarse $d_{50} = 25\,\mu m$ powders with a BET surface area of $0.4\,m^2/g$, medium $d_{50} = 7\,\mu m$ powders with a BET surface area of $1.2\,m^2/g$ and fine $d_{50} = 2\,\mu m$ powders with a BET surface area of $6.0\,m^2/g$. According to the manufacturer's information, all three powders contained impurities of 0.07 wt.% Fe, 0.07 wt.% Al, 0.01 wt.% Ca, 0.1 wt.% C and 0.2–1.0 wt.% O (oxygen content was dependent on the particle size distribution). The oxygen contents measured by an oxygen/nitrogen analyzer (LECO) were 0.27 wt.% for the average particle size of 25 μm, and 0.56 and 1.9 wt.% for the average particle sizes of 7 and 2μm, respectively. The average particle size was confirmed by a Coulter LS particle size analyzer and a Hitachi S-2400 Scanning Electron Microscope.

Y_2O_3 (H.C. Starck, fine grade) and Al_2O_3 (Sumitomo Chemical AKP-30) were used mainly as sintering additives. Addition contents were 6 wt.% Y_2O_3 and 1 wt.% Al_2O_3 (6Y1A) for the primary experiments of size comparison. In the case of the densification experiment of coarse 25 μm powders, additive systems were modified. Since coarse 25 μm powders had less SiO_2 content than 2 or 7 μm powders, more SiO_2 (Cerac −325 mesh, 99.5% pure) was added to be the composition of 6 wt.% Y_2O_3 + 1 wt.% Al_2O_3 + 2 wt.% SiO_2 (6Y1A2S). As it is known that Al_2O_3 decreases the viscosity of the liquid phase, more Al_2O_3 has been added to the additive system of 6 wt.% Y_2O_3 + 3 wt.% Al_2O_3 + 2 wt.% SiO_2 (6Y3A2S) [9,15,16]. In order to compare the effect of the amount of liquid phase, the total amount of additives was increased to be the composition of 9 wt.% Y_2O_3 + 1.5 wt.% Al_2O_3 + 3 wt.% SiO_2 (9Y1.5A3S).

Fig. 1 shows the schematic flow diagram of experimental procedure. Si powders with sintering additives and 1 wt.% PEG 300 as a binder were mixed for 12 h in a plastic jar using Si_3N_4 balls in ethanol. They were dried while stirring at 40–50 °C on a hot plate. The dried powder mixture were sieved to −80 mesh to approximately +140 mesh, and pressed uniaxially into the disk-shaped compacts of 30 mm diameter under 50 MPa. After compaction, the PEG 300 binder was burnt out to enhance the pore-channel

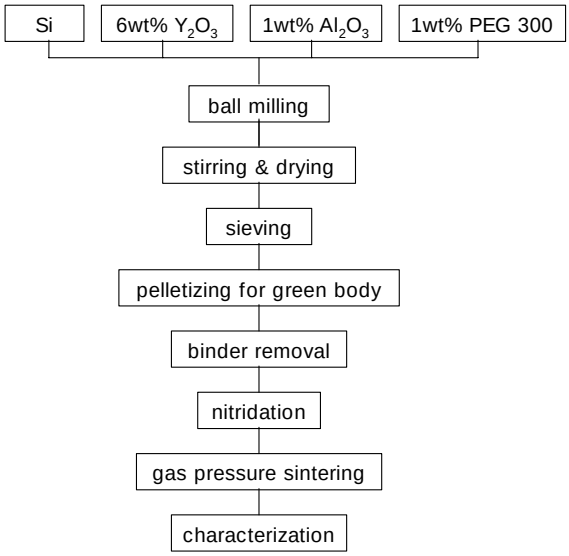

Fig. 1. Schematic flow diagram of experimental procedure. Sintering additives of 6Y1A was changed in the densification experiments of coarse powders.

distribution in the green compacts. The burn-out process was done at 600 °C for 1 h under a flowing N_2 atmosphere.

After the binder burn-out operation, the compacts were subjected to nitridation in a tube furnace with a quasi-static 95% N_2/5% H_2 gas mixture, controlled at a positive pressure of 20 kPa. It was essentially a gas demanding system wherein the temperature was regulated by a signal from a pressure transducer. As the nitriding reaction proceeds, nitrogen is consumed and the furnace pressure drops below the control pressure. Nitriding gas is then allowed to enter the furnace to maintain the constant control pressure of 120 kPa. Simultaneously, temperature is held for a minimum time to allow the reaction to approach equilibrium. The nitridation was done as the multi-step process up to 1450 °C during 29.5 h. The holding time at the maximum nitridation temperature of 1450 °C was 2 h. After the nitridation process the percent of nitridation and the relative density were measured. The percent of nitridation was calculated from the weight change before and after nitridation. The relative density was calculated from the theoretical density and the sintered density was obtained from the weight and dimension measurement.

Postsintering was performed in a gas-pressure-sintering furnace (Ionex, USA) under different N_2 gas pressures. The postsintering temperatures were 1550–1850 °C with intervals of 100, 1900 and 1950 °C. It was done at 1550–1750 °C for 0.5 h under 1 MPa N_2 pressure, at 1850 °C for 0.5 and 3 h under 2 MPa N_2 pressure, and at 1900 and 1950 °C for 3 h under 2 MPa N_2 pressure.

To identify the phases and to do the quantitative phase analysis, XRD was performed on the cross-section of the sintered specimens by using a Rigaku D/MAX 2200 diffractometer.

The fracture strength was measured on the bar samples 3 mm × 4 mm × 25 mm in a three-point bending fixture with a span of 20 mm and a crosshead speed of 0.5 mm/min (Instron 2406). The surfaces of the bars were machined and then polished with diamond paste down to 1 μm. The fracture toughness was measured on the polished surfaces by the indentation crack length method using 196 N load with a Vickers hardness tester (Mitutoyo AVK-C2). To obtain the fracture toughness value Evans and Charles' equation [17] was used.

For microstructural investigation, the cross-section of the polished specimens was plasma-etched using a mixture of CF_4 with 5% oxygen for 4 min. The samples were then Au-coated and examined with scanning electron microscopy (SEM).

3. Results and discussion

The percent of nitridation and the relative density of the specimens reaction sintered at 1450 °C with different particle size powders are shown in Fig. 2. An average of seven specimens was taken. The specimens using coarse 25 μm

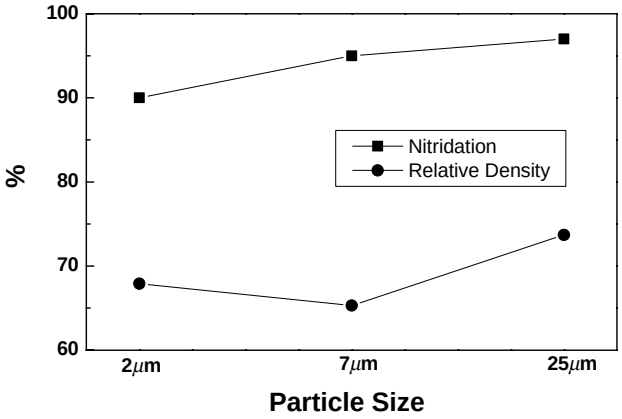

Fig. 2. Percent of nitridation and relative density of the specimens reaction sintered with different particle size powders.

powders show 97% nitridation, while the specimens using medium 7 μm powders and fine 2 μm powders show 95 and 90% nitridation, respectively. The nitridation rate increases apparently with increasing particle size. The relative densities, however, show the fluctuation in change from 73.7% for coarse 25 μm powders to 65.3% for 7 μm powders.

The increase of the nitridation rate with increasing particle size is probably due to the decrease in SiO_2 content on the starting Si powders. The oxygen contents measured by the oxygen/nitrogen analyzer were 1.9, 0.5 and 0.27 wt.% in the cases of 2, 7 and 25 μm, respectively. The amount of SiO_2 converted from these oxygen contents is 3.56, 1.05 and 0.51 wt.%, respectively. Thus, in the specimens using coarse 25 μm powders a small amount of liquid phase is formed, and there is a less possibility of a blocking of the pore-channel structures. The existence of the continuous pore-channel structures in the nitridation process is thought to improve the diffusion of N_2 gas, which then enhances the nitridation rate. Thus, the enhanced nitridation rate would be expected in the specimens using coarse 25 μm powders, which seems to be due to a smaller amount of liquid phase and large pore-channel structures in the compacts.

Fig. 3 shows the XRD patterns on the cross-section of the specimens reaction sintered at 1450 °C with different particle size powders. All patterns have the peaks due to α- and β-Si_3N_4 as the major phases. However, the distinct difference in the secondary phases is shown on three patterns, although all specimens were prepared under identical nitridation conditions and identical additives of 6 wt.% Y_2O_3 + 1 wt.% Al_2O_3 were used. It is noticeable that the specimens using fine 2 μm powders, medium 7 μm powders and coarse 25 μm powders show the appearance of α-$Y_2Si_2O_7$ phase, $Y_{10}Si_6O_{24}N_2$ phase and $YSiO_2N$ phase, respectively.

Pseudoquaternary phase equilibrium diagram for the system Si-Y-O-N [18] is shown in Fig. 4. As shown in the figure, if yttrium content (*x*-axis) is fixed, Si_3N_4 phase is compatible with $Y_2Si_2O_7$ phase, $Y_{10}Si_6O_{24}N_2$ phase, $YSiO_2N$ phase and $Y_2Si_3O_3N_4$ phase with decreasing oxygen content.

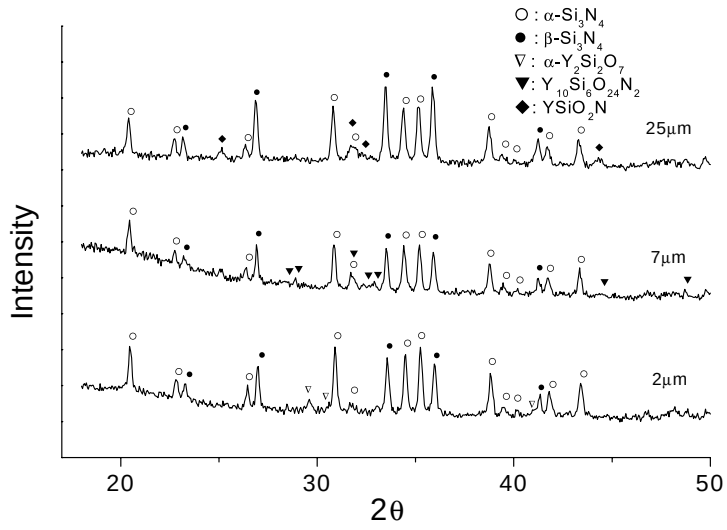

Fig. 3. XRD patterns on the cross-section of the specimens reaction sintered with different particle size powders.

This supports the fact that in the case of fine 2 μm powders containing more SiO_2 content $Y_2Si_2O_7$ phase dominantly appears as the secondary phase, and $Y_{10}Si_6O_{24}N_2$ phase dominantly appears in medium 7 μm powders containing less SiO_2 content. Also, the appearance of $YSiO_2N$ phase is found in the case of coarse 25 μm powders containing much less SiO_2 content. At this point Y Eq.% has somewhat higher value in fine powders, but it is approximately calculated to be 1.8–1.85 Eq.%. Increasing oxygen content of the Si powder favors the precipitation of phases lowering the Y/O ratio.

Fig. 5 shows the relative densities of the specimens gas-pressure sintered at different sintering temperatures. The specimens using coarse powders exhibit higher densification in lower temperature regions of the figure, but the tendency disappears at higher temperatures. In higher temperature regions the specimens using fine powders exhibit higher densification. Higher densification of the specimens using coarse 25 μm powders in lower temperature regions may be due to the role of pore channel similar to the nitridation behavior of Fig. 2. The lower value of 90% in relative density, however, was obtained in the specimen sintered at 1850 °C for 3 h by using 25 μm powders. This is probably due to the abnormal growth of elongated β-phase grain created by the insufficient amount of the liquid phase.

In the case of coarse 25 μm powders, the amount of SiO_2 content is small and the spread of a liquid phase is not good. Thus, phase transformation and grain growth selectively

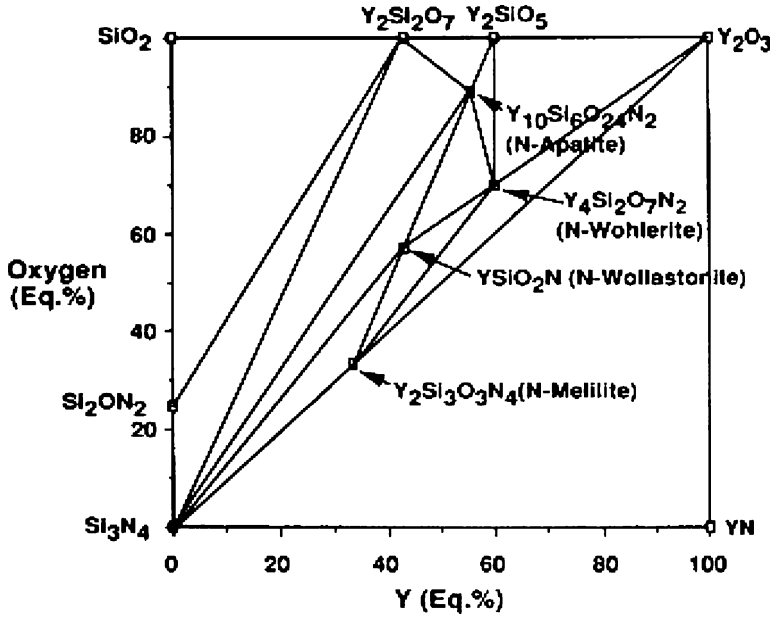

Fig. 4. Pseudoquaternary phase equilibrium diagram for the system Si-Y-O-N [18].

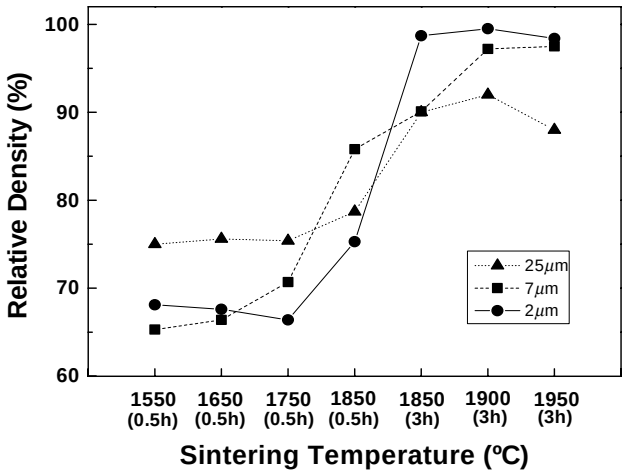

Fig. 5. Relative densities of the specimens gas-pressure sintered at different sintering temperatures.

occur near the liquid-phase parts, and then the growth occurs fast due to the mass transport from many non-transformed grains. β-Phases, well developed at low temperatures, become abnormally larger with increasing sintering temperature and a decline in density is shown in higher temperature regions.

However, in the case of fine powders the densification near the theoretical density is shown. This may be attributed to the appropriate amount and the good spread of the liquid phase, which gives rise to the uniform phase transformation all over the specimens.

Fig. 6 shows the XRD patterns on the cross-section of the specimens gas-pressure sintered at different sintering temperatures after reaction sintering with different particle size powders. The XRD pattern on the specimens reaction sintered at 1450 °C is also shown for reference. At 1450 °C, each pattern has the peaks of the secondary phase in addition to the peaks due to α- and β-Si_3N_4, as mentioned above.

In Fig. 6a used fine 2 μm powders, three phases of α-$Y_2Si_2O_7$ phase, α-Si_3N_4 phase and β-Si_3N_4 phase are shown at 1450 °C. At 1550 °C, these phases exist, but the relative increase in β-phase and the decrease in α-phase are shown. α-$Y_2Si_2O_7$ phase exists up to 1650 °C, but it does not appear above this temperature. Also, α-phase exists up to 1650 °C and only β-phase exists above 1750 °C.

In the cases of 7 and 25 μm powders, the behavior of phases on temperature is similar to that of 2 μm powders, except for the secondary phase. $Y_{10}Si_6O_{24}N_2$ phase appeared in the specimens using 7 μm powders exists up to 1750 °C (Fig. 6b). However, in the case of coarse 25 μm powders $YSiO_2N$ phase exists up to 1650 °C and another phase, $Y_2Si_3O_3N_4$, appears at 1750 °C (Fig. 6c).

It is expected that the secondary phases are precipitated from the Y-Si-Al-O-N oxynitride glass consisting of Si_3N_4, SiO_2, Y_2O_3 and Al_2O_3, because the nitridation was done at 1450 °C, which is higher than the eutectic temperature (1370 °C) in the system Y_2O_3-Al_2O_3-SiO_2 [19]. The oxynitride secondary phases, α-$Y_2Si_2O_7$, $Y_{10}Si_6O_{24}N_2$ and $YSiO_2N$, precipitated in the nitridation process persist up to 1650–1750 °C, but they are melted at the higher temperatures. Thus, their existence was not shown in the XRD patterns. In the case of 25 μm powders, the existence of $YSiO_2N$ phase up to 1650 °C and new appearance of $Y_2Si_3O_3N_4$ phase at 1750 °C may be explained as follows.

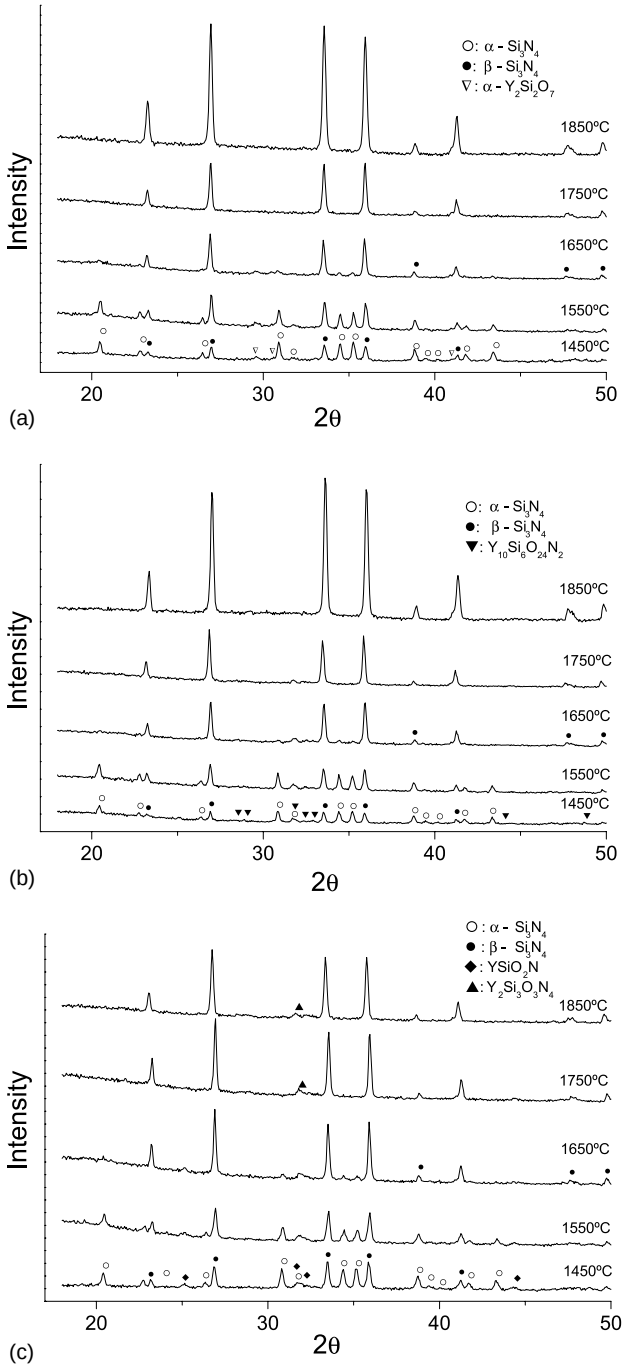

Fig. 6. XRD patterns on the cross-section of the specimens gas-pressure sintered at different sintering temperatures after reaction sintering with different particle size powders: (a) 2 μm, (b) 7 μm and (c) 25 μm.

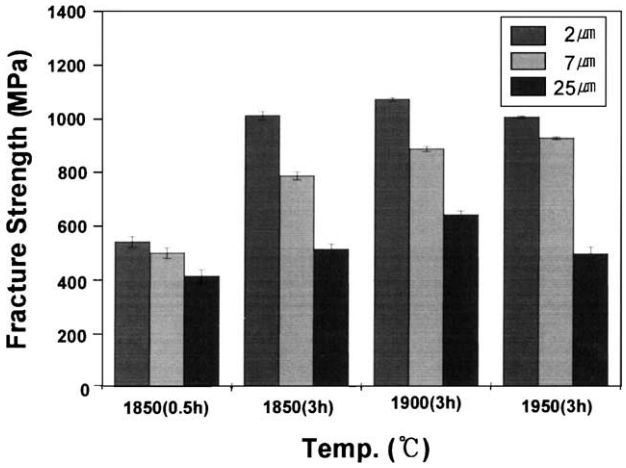

Fig. 7. Fracture strengths of the specimens gas-pressure sintered at different sintering temperatures.

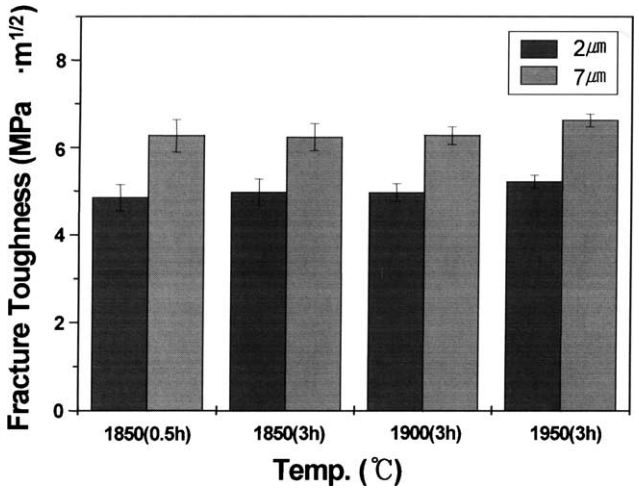

Fig. 8. Fracture toughnesses of the specimens gas-pressure sintered at different sintering temperatures.

It seems that oxygen content in the system up to 1650 °C is low enough to produce wollastonite ($YSiO_2N$). However, with further loss in oxygen content and a change in the glass composition due to the melting of wollastonite phase with increasing temperature, the melilite ($Y_2Si_3O_3N_4$) phase is precipitated.

The fracture strengths of the specimens gas-pressure sintered at different temperatures are shown in Fig. 7. An average of five specimens was taken. In the case of fine 2 μm powders, a lower value of fracture strength is shown at 1850 °C for 0.5 h, reflecting a lower density of Fig. 5. However, the relatively high fracture strengths of above 1 GPa are obtained from the other sintering conditions, reflecting the high densities near the theoretical density. The strength values of the specimens using medium 7 μm powders are generally lower than those using fine 2 μm powders, and the increase in strength with increasing sintering temperature is shown. Very lower strengths are observed in the specimens using coarse 25 μm powders, reflecting the low densities of below 90%.

Also the variation of micro-Vickers hardness was measured. The observed variation in hardness was a direct consequence of the variation in strength and density. It is noticeable that as the particle size decreases, a higher value in strength and hardness is observed.

Fig. 8 shows the fracture toughnesses of the gas-pressure-sintered specimens. For the measurement of the fracture toughness two specimens were used, and an average of the values measured seven times was taken. In the case of fine 2 μm powders, a fracture toughness of 4.5–5.0 MPa $m^{1/2}$ was obtained. However, the relatively high toughness of 6.0–6.5 MPa $m^{1/2}$ was obtained in specimens using medium 7 μm powders. Specimens using 7 μm powders show toughnesses higher of about 20% than the specimens obtained using 2 μm powders. There are reports [20–22] that the value of fracture toughness is related to the diameter of the large grains. It is expected that the diameter of the grains on microstructure becomes large on the specimens using 7 μm powders (refer Figs. 9 and 10).

A study on microstructure was done by SEM observation. Figs. 9 and 10 show the SEM micrographs of the specimens gas-pressure sintered at 1850 and 1900 °C for 3 h, respectively. The development of elongated grains is shown with increasing particle size. As the sintering temperature increases, the elongated grains develop much more also and the dense structure reflecting higher densification is shown.

In the case of coarse 25 μm powders, the higher densification shown at the nitridation temperature and lower postsintering temperatures may be due to the improvement of pore-channel structure, but the decrease in density becomes apparent by higher postsintering temperatures. In the case of 25 μm powders, new melilite phase appeared at 1750 °C and existed above temperatures in succession. Because of the decrease in liquid-phase contents this will be a cause of the low density at higher sintering temperatures. The melting point of $Y_2Si_3O_3N_4$ phase is known at ~1900 °C [23]. The insufficiency in liquid-phase contents results in lower densification, but it has a great influence on the growth of elongated grains. The decrease in density resulted in the decrease in strength and hardness.

However, in the case of fine 2 μm powders the densification near the theoretical density at higher postsintering temperatures was shown because of the appropriate amount and the good spread of the liquid phase. The high density resulted in high strength and hardness. The liquid phase is already formed below 1450 °C, and the amount of liquid phase decreases with precipitating the oxynitride crystalline phase. At higher temperatures the oxynitride phase melts and densification near the theoretical density is then obtained. The melting point of $Y_2Si_2O_7$ phase is known at 1790 °C [19,23]. What is called the transient liquid-phase sintering is occurred [24,25]. This is supported by a fact that the specimens using 2 μm powders cannot attain the high density in lower postsintering temperatures, but the

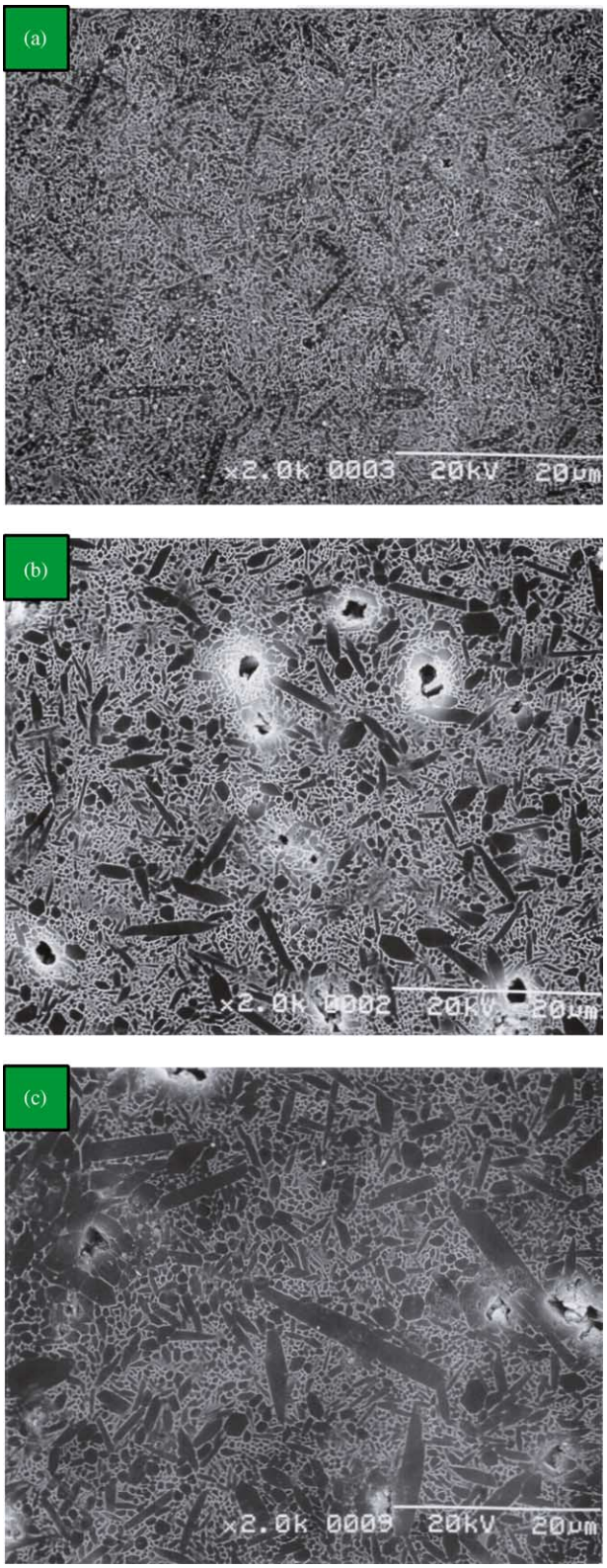

Fig. 9. SEM micrographs of the specimens gas-pressure sintered at 1850 °C for 3 h: (a) 2 μm, (b) 7 μm and (c) 25 μm.

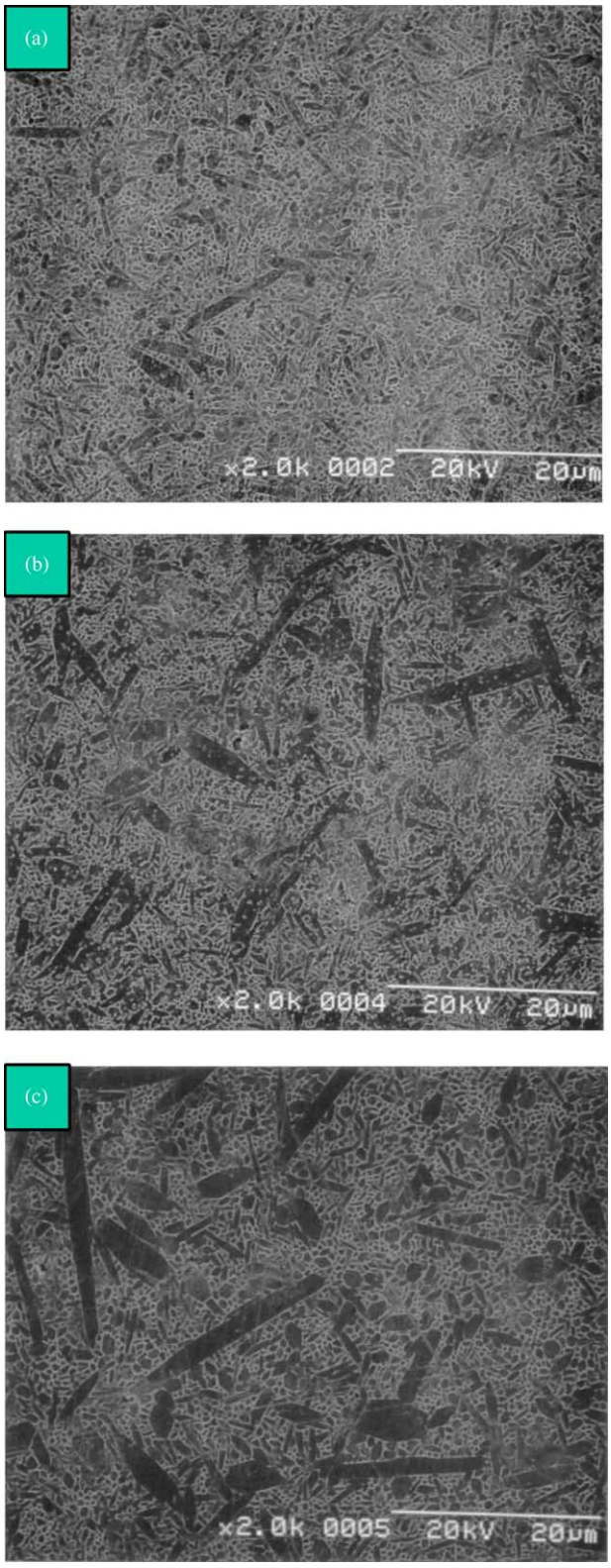

Fig. 10. SEM micrographs of the specimens gas-pressure sintered at 1900 °C for 3 h: (a) 2 μm, (b) 7 μm and (c) 25 μm.

Table 1
Compositions of sintering additives for coarse 25 μm powders

Notation	Weight fraction		
	Y_2O_3	Al_2O_3	SiO_2[a]
6Y1A	6 (0.82)	1 (0.14)	0.51 (0.04)
6Y1A2S	6 (0.64)	1 (0.11)	2.51 (0.25)
6Y3A2S	6 (0.53)	3 (0.27)	2.51 (0.20)
9Y1.5A3S	9 (0.65)	1.5 (0.11)	3.51 (0.24)

[a] SiO_2 content of 25 μm Si powders is 0.51 wt.%.

rapid densification is attained at 1850 °C for 3 h, as shown in Fig. 5. Since the densification processes are thermally activated processes, the time may be needed to make a rearrangement process at a high temperature. The rapid increase in density is shown in the holding time of 3 h than 0.5 h at 1850 °C.

Fine grained specimens possess a higher fracture strength but a relatively lower fracture toughness. However, for 7 μm powders consisting of bimodal structure the improvement in fracture toughness is remarkable. In the specimens sintered at 1900 °C using 7 μm powders, fracture strength of 880 MPa and fracture toughness of 6.3 MPa $m^{1/2}$ were obtained.

The lower value of 90% in relative density was obtained in the specimen sintered at 1850 °C for 3 h by using 25 μm powders. Such a lower densification persisted up to higher temperatures. Therefore, we tried to improve the densification using different sintering additives. The various sintering additives, such as 6 wt.% Y_2O_3 + 1 wt.% Al_2O_3 + 2 wt.% SiO_2 (6Y1A2S), 6 wt.% Y_2O_3 + 3 wt.% Al_2O_3 + 2 wt.% SiO_2 (6Y3A2S) and 9 wt.% Y_2O_3+1.5 wt.% Al_2O_3+3 wt.% SiO_2 (9Y1.5A3S), were used in order to investigate the densification behavior, as shown in Table 1.

Fig. 11 shows the nitridation rate on the specimens reaction sintered with different sintering additives. The specimens using 6Y1A show 97% nitridation, while the specimens using 6Y1A2S added more SiO_2 content show 94% nitridation. A decline in nitridation to below 90% is shown in 6Y3A2S and 9Y1.5A3S which contained more sintering additives.

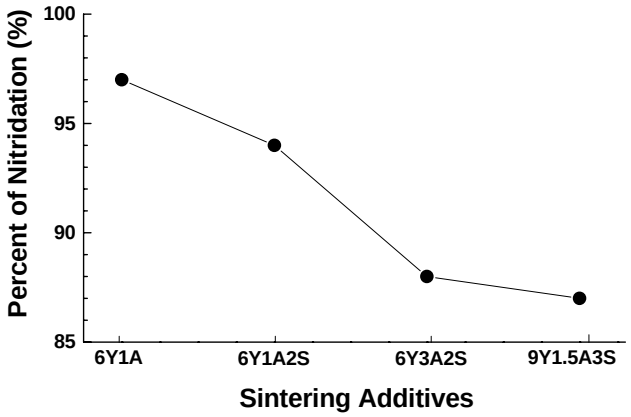

Fig. 11. Percent of nitridation of the specimens reaction sintered with different sintering additives.

6Y1A2S is the system where 2 wt.% SiO_2 is added to 6Y1A. This SiO_2 content is the same amount with the content difference in native oxides between 2 and on 25 μm powders. Thus, if we add 6Y1A2S on 25 μm powders, the SiO_2 content is the same as 6Y1A system on 2 μm powders. However, higher nitridation rate was shown in the 6Y1A2S addition on 25 μm powders (94% in 25 μm Si powders + 6Y1A2S, 90% in 2 μm Si powders + 6Y1A), because the diffusion of nitrogen gas through the pore-channel structure has a great influence in the compacts using coarse powders. As the amount of sintering additives increased, the percent nitridation drops. This may be also due to the decrease in nitrogen diffusion through the pore-channel structure, owing to the increase in liquid-phase contents.

Postsintering on 25 μm powders with different sintering additives was done at 1850 and 1900 °C for 3 h under 2 MPa N_2 pressure. We investigated the densification behavior on the samples added 2 wt.% SiO_2 content on 25 μm Si powders + 6Y1A, but high densification was not attained even at high temperatures. This contrasts with a high densification on 2 μm Si powders + 6Y1A, expected to contain the same liquid-phase contents. The poor densification on 25 μm Si powders+6Y1A2S is probably due to the inhomogeneous distribution of the liquid phase. It is expected that in the case of fine powders SiO_2 exists on each powder with a homogeneous distribution, but the SiO_2 addition on coarse powders will be a cause of an inhomogeneous distribution.

Accordingly, the additives altered in addition amount and composition, such as 6Y3A2S and 9Y1.5A3S, were added. In both cases, high densities near the theoretical density were obtained. Contrary to the low density of 90% in 6Y1A, in the case of 6Y3A2S high densities of 98 and 99.9% were obtained at 1850 and 1900 °C, respectively. The values of density at 1850 and 1900 °C in 9Y1.5A3S were 93 and 99.5%, respectively. This result is attributed to the increase in liquid-phase contents.

In the case of 9Y1.5A3S the low density of 93% at 1850 °C seems to be due to the composition of additives. As compared with 6Y1A2S, in the case of 9Y1.5A3S the total amount of sintering additives is increased one and half times, but the composition is nearly the same. Also, a low density of 83% was obtained in 6Y1A2S. From these we may be able to guess that the additive composition of 9Y1.5A3S did not form enough liquid phase of a lower viscosity at 1850 °C. However, in the case of 9Y1.5A3S at 1900 °C a densification near the theoretical density was obtained. From this we may be able to guess that the viscosity of liquid phase was sufficiently lowered at the sintering temperature of 1900 °C, thus allowing full densification.

Fig. 12 shows the XRD patterns on the cross-section of the specimens gas-pressure sintered at 1850 °C with different sintering additives. As shown in Fig. 6c, in the case of 6Y1A melilite phase existed at 1850 °C, and it was then a cause of the insufficiency in liquid-phase contents. However, in the

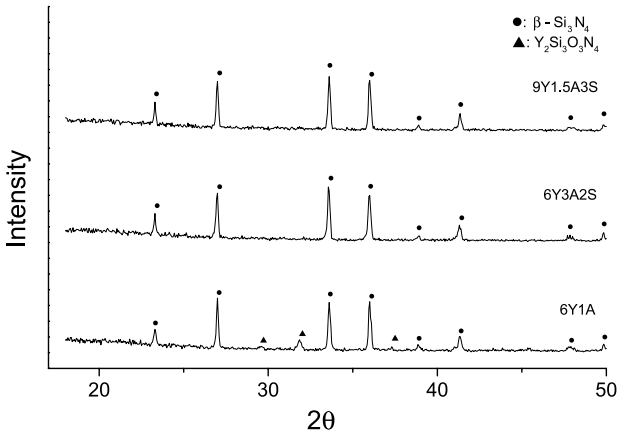

Fig. 12. XRD patterns on the cross-section of the specimens gas-pressure sintered at 1850 °C with different sintering additives.

cases of 6Y3A2S and 9Y1.5A3S the secondary phase was not detected on the XRD patterns of the samples sintered at 1850 and 1900 °C. This result is attributed to an offer of the sufficient oxygen in 6Y3A2S and 9Y1.5A3S.

The variation of fracture strength with sintering additives is shown in Fig. 13. Fracture strength in 6Y1A is also shown for reference. Very low strengths are observed in 6Y1A, reflecting lower densities of below 90%. However, the relatively high fracture strengths of 850–960 MPa are obtained in 6Y3A2S and 9Y1.5A3S, reflecting the high densities near the theoretical density. The increase in strength is shown with increasing sintering temperature. A lower value of strength is observed in 9Y1.5A3S at 1850 °C, reflecting a lower density of 93%. The variation in hardness was also a direct consequence of the variation in strength and density. As the amount of liquid phase increases, an increase in hardness also occurred.

The variation of fracture toughness with sintering additives is shown in Fig. 14. Fracture toughness values of about 6.5 MPa $m^{1/2}$ are shown. A high fracture toughness

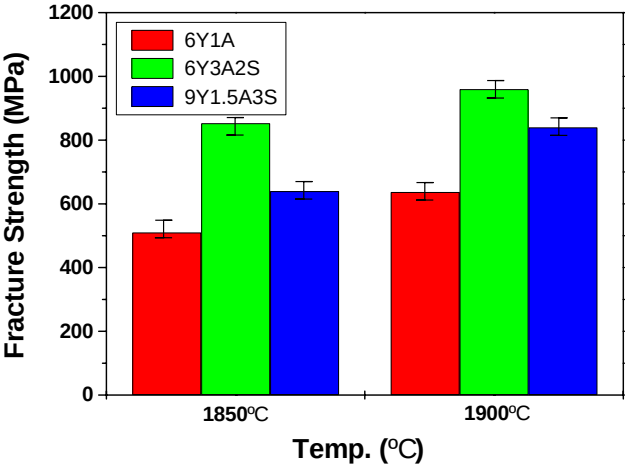

Fig. 13. Variation of fracture strength with sintering additives for the specimens gas-pressure sintered at 1850 and 1900 °C.

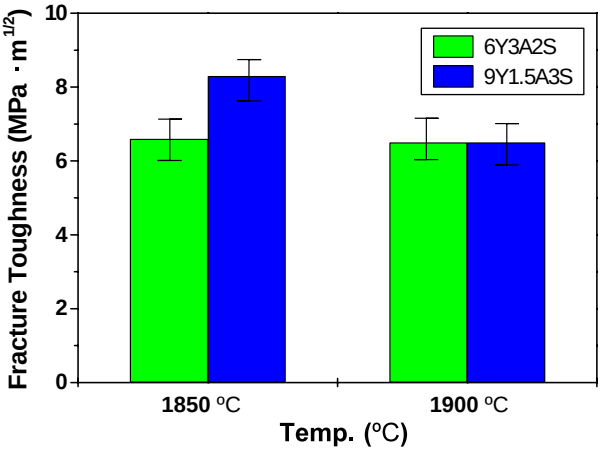

Fig. 14. Variation of fracture toughness with sintering additives for the specimens gas-pressure sintered at 1850 and 1900 °C.

in 9Y1.5A3S at 1850 °C is probably due to a relatively low density.

Figs. 15 and 16 show the SEM micrographs of the specimens gas-pressure sintered at 1850 and 1900 °C for 3 h, respectively. SEM micrographs of 6Y1A already suggested in Figs. 9c and 10c are presented again in panel 'a' of figures for comparison. The development of elongated grains is shown in Fig. 15a of 6Y1A addition. However, in the case of 6Y3A2S which Al_2O_3 contents in the sintering additives is increased (Fig. 15b), the size of coarse elongated grains gets small and the number of elongated grains increases. These results are consistent with the report of Ziegler et al. [9] in which a small number of coarse elongated grains is formed with decreasing amount of liquid phase and with increasing viscosity. As the amount of liquid phase gets small and the viscosity is increasing, local densification occurs and the large grains continuously grow owing to Ostwald ripening. Thus, a small number of coarse elongated grains are formed.

A similar phenomenon is also observed in Fig. 16 at increased sintering temperature. As the temperature increases, the elongated grains are developed much more. The development of coarse elongated grains is shown in Fig. 16a. The variation in the development of elongated grains with sintering additives has the similar tendency to Fig. 15. All the SEM micrographs show the microstructures to correspond to the variation in density and fracture toughness with sintering additives.

The specimens using 25 μm Si powders + 6Y1A showed the low values in density and strength, because of the abnormal growth of elongated β-Si_3N_4 grains owing to the insufficiency and the inhomogeneous distribution in liquid phase. If the amount of liquid phase is small, the degree of phase transformation and grain growth becomes different locally in the specimen depending on the distribution of liquid phase. Fastly grown grains become larger due to the mass transport around small grains. Such a fast grain growth of inhomogeneous and coarse elongated grains was the cause of a decline in density and strength.

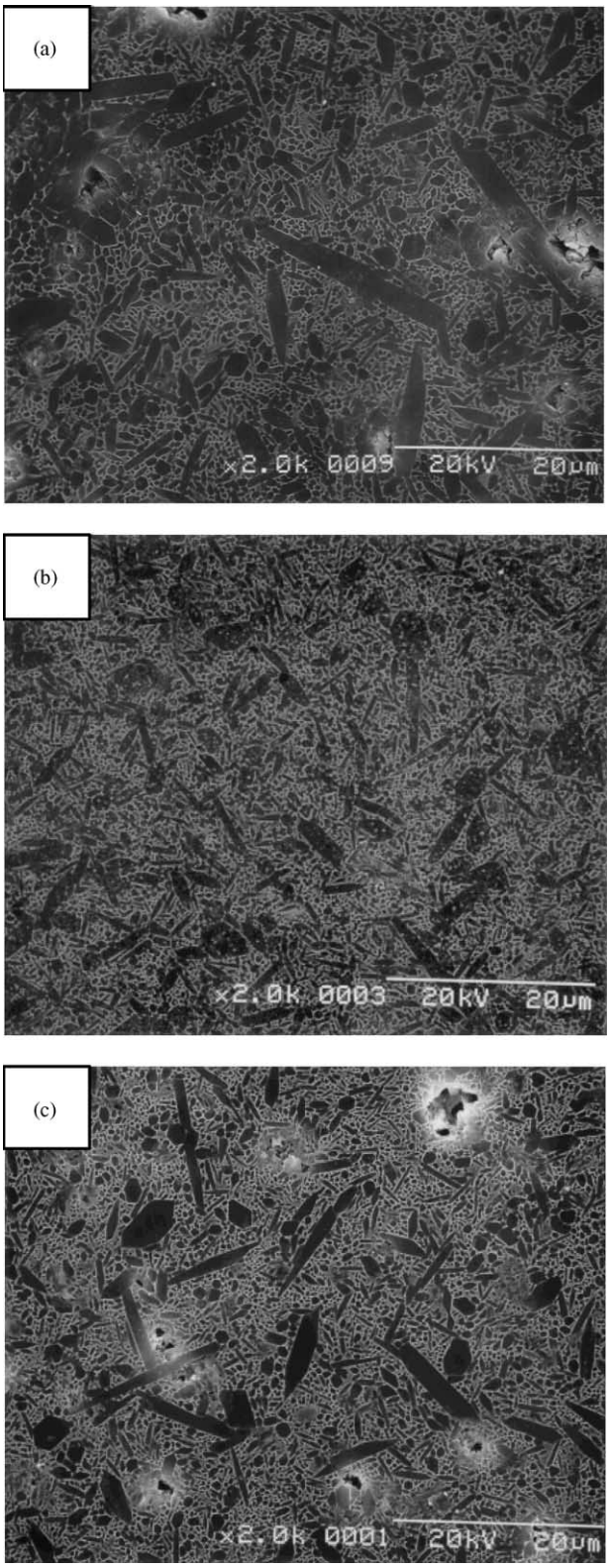

Fig. 15. SEM micrographs of the specimens gas-pressure sintered at 1850 °C with sintering additives: (a) 6Y1A, (b) 6Y3A2S and (c) 9Y1.5A3S.

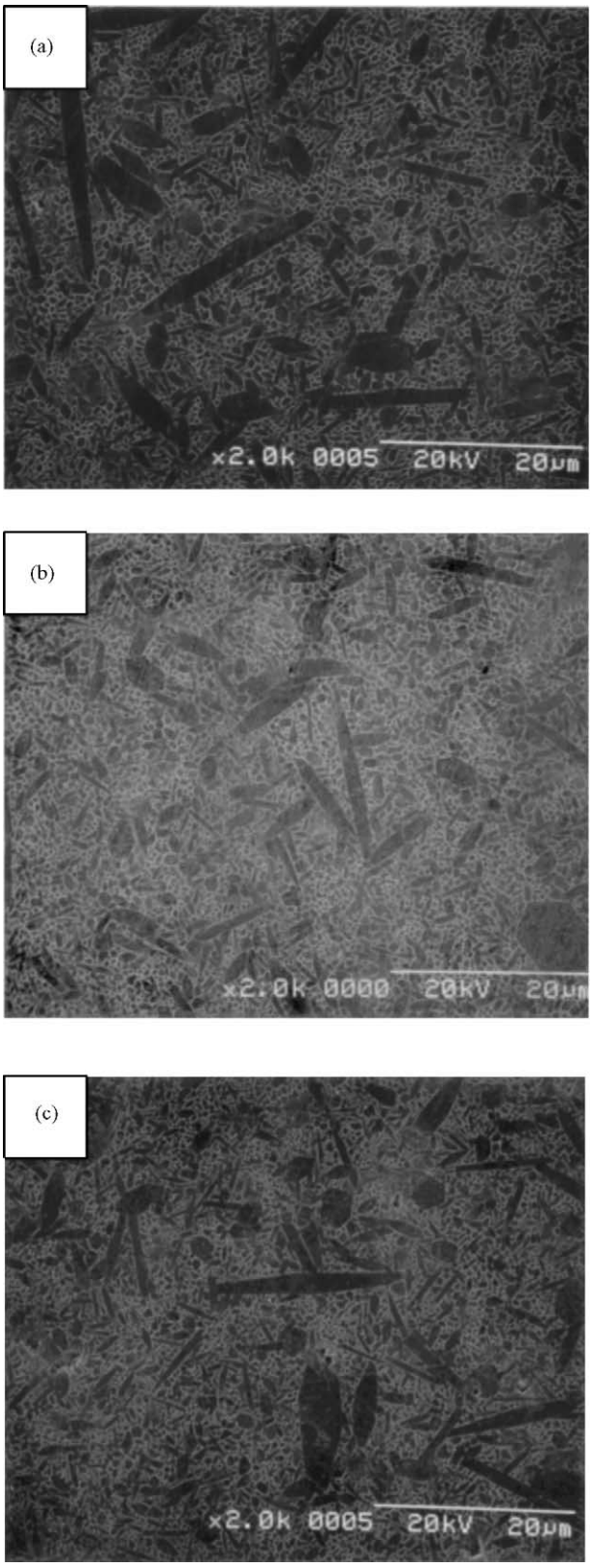

Fig. 16. SEM micrographs of the specimens gas-pressure sintered at 1900 °C with sintering additives: (a) 6Y1A, (b) 6Y3A2S and (c) 9Y1.5A3S.

However, the specimens using more additive contents, such as 6Y3A2S and 9Y1.5A3S, showed an increase in density and strength owing to an appropriate amount and a good spread of liquid phase. In the case of 6Y1A a low fracture strength of 637 MPa was obtained at 1900 °C, but the fracture strength increased up to 960 MPa in 6Y3A2S addition.

The specimens using 2 μm Si powders + 6Y1A showed fracture strengths of above 1 GPa and a fracture toughness of 4.5–5.0 MPa $m^{1/2}$ as discussed above. The specimens using 7 μm Si powders + 6Y1A showed a fracture strength of 800–900 MPa and a fracture toughness of 6.0–6.5 MPa $m^{1/2}$. In the specimens sintered at 1900 °C using 25 μm Si powders + 6Y3A2S, a high fracture strength of 960 MPa and a fracture toughness of 6.5 MPa $m^{1/2}$, however, were obtained. These are similar values and/or more balanced values in comparison with the values obtained by using more finer 2 and 7 μm Si powders. Since the coarse Si powders are much cheaper than the fine Si powders, the economical impact in manufacturing Si_3N_4 ceramics is expected.

4. Conclusions

The effect of raw-Si particle size on the property of sintered RBSN was investigated by the use of Si powders with different particle sizes containing various native oxide SiO_2 contents.

The specimens reaction sintered at 1450 °C with coarse Si powders showed higher nitridation than those using fine Si powders, due to the increase of nitrogen gas diffusion through the pore-channel structure. The different secondary phases were formed at each specimens reaction sintered with different particle sizes. The specimens using fine 2 μm powders, medium 7 μm powders and coarse 25 μm powders showed the appearance of α-$Y_2Si_2O_7$ phase, $Y_{10}Si_6O_{24}N_2$ phase and $YSiO_2N$ phase, respectively. This was due to the content difference in native oxide on the surface layer of particles, and was a qualitatively corresponding result in the phase equilibrium diagram for the system Si-Y-O-N.

In the case of coarse 25 μm powders $YSiO_2N$ phase was precipitated after nitridation, but $Y_2Si_3O_3N_4$ phase was precipitated with increasing postsintering temperature. The densification was not performed at even high temperatures because of the abnormal growth of elongated β-Si_3N_4 grains owing to the insufficiency and the inhomogeneous distribution of the liquid phase occurred from the precipitation of the oxynitride crystalline phase. The low densification resulted in the low value of strength.

However, the specimens using fine 2 μm powders showed a rapidly increased densification at 1850 °C. The increased densification was due to the supply of enough amount of liquid phase by the melting of the $Y_2Si_2O_7$ phase. The microstructure consist of fine β-Si_3N_4 grains and the dense structure. A low fracture toughness of about 5 MPa $m^{1/2}$ was obtained, but the fracture strength had a high value of above 1 GPa.

In the case of medium 7 μm powders the densification was suppressed up to 1750 °C due to the decrease in the amount of liquid phase by the precipitating of $Y_{10}Si_6O_{24}N_2$ phase. However, the densification was rapidly occurred above 1750 °C due to the supply of a liquid phase by the melting of the $Y_{10}Si_6O_{24}N_2$ phase. At 1900 °C the high densification of 97% TD was performed, and the bimodal structure was shown on microstructure. A fracture strength of 880 MPa weakened the decrease in strength and a fracture toughness of 6.3 MPa $m^{1/2}$ improved the toughness were obtained on the bimodal structure.

Higher values of fracture strength were obtained for the specimens using fine powders, however, higher values of fracture toughness were obtained when large elongated grains are developed in a fine grained matrix.

To improve the values of density and strength in the specimens using coarse 25 μm powders, different sintering additives were also added. Densification near the theoretical density was attained by using the sintering additives, such as 6 wt.% Y_2O_3 + 3 wt.% Al_2O_3 + 2 wt.% SiO_2 (6Y3A2S) and 9 wt.% Y_2O_3 + 1.5 wt.% Al_2O_3 + 3 wt.% SiO_2 (9Y1.5A3S).

In the case of 6Y3A2S addition, a high fracture strength of 960 MPa and a fracture toughness of 6.5 MPa $m^{1/2}$ were obtained. These were similar values and/or more balanced values in comparison with the values obtained by using finer powders. Full densification and promotion of mechanical properties for the preparation of RBSN by using coarse Si powders will exert a beneficial influence on a manufacturing process of silicon nitride ceramics.

Acknowledgements

This article was financially supported by the RCEC of Dongeui University.

References

[1] L.J. Schioler, Heat engine ceramics, Am. Ceram. Soc. Bull. 64 (2) (1985) 268–294.
[2] A. Giachello, P. Popper, Post-sintering of reaction-bonded silicon nitride, Ceram. Int. 5 (3) (1979) 110–114.
[3] J.A. Mangels, Sintered reaction-bonded silicon nitride, Ceram. Eng. Sci. Proc. 2 (1982) 589–603.
[4] A. Atkinson, P.J. Leatt, A.J. Moulson, E.W. Roberts, A mechanism for the nitridation of silicon powder compacts, J. Mater. Sci. 9 (1974) 981–984.
[5] D.P. Elias, M.W. Lindley, Reaction sintered silicon nitride, J. Mater. Sci. 11 (1976) 1278–1295.
[6] A.J. Moulson, Reaction-bonded silicon nitride: its formation and properties, J. Mater. Sci. 14 (1979) 1017–1051.
[7] H.M. Jennings, On reaction between silicon and nitrogen, J. Mater. Sci. 18 (1983) 951–967.
[8] H. Kim, C.H. Kim, The influence of the various transport properties of the nitriding atmosphere on the formation of reaction-bonded Si_3N_4, J. Mater. Sci. 20 (1985) 141–156.
[9] G. Ziegler, J. Heinrich, G. Wotting, Relations between processing, microstructure and properties of dense and reaction-bonded silicon nitride, J. Mater. Sci. 22 (1987) 3041–3086.

[10] J.A. Mangels, The effect of silicon purity on the strength of reaction-bonded Si_3N_4, J. Mater. Sci. Lett. 15 (1980) 2132–2135.
[11] H.J. Kleebe, G. Ziegler, Influence of crystalline secondary phases on the densification behavior of reaction-bonded silicon nitride during postsintering under increased nitrogen pressure, J. Am. Ceram. Soc. 72 (12) (1989) 2314–2317.
[12] W.B. Li, B.Q. Lei, T. Lindback, A kinetic model for reaction bonding process of silicon powder compact, J. Eur. Ceram. Soc. 17 (1997) 1119–1131.
[13] S. Wada, Increase of oxygen content in Si_3N_4 powder during ball milling using alcohol as solvent, J. Ceram. Soc. Jpn. 104 (11) (1996) 1085–1087.
[14] H.D. Kim, E.Y. Sun, P.F. Becher, H.J. Kim, B.D. Han, D.S. Park, Effect of increased oxygen content due to intensive milling on phase and microstructural development of silicon nitride, J. Kor. Ceram. Soc. 38 (5) (2001) 405–411.
[15] A. Kuzjukevics, K. Ishizaki, Sintering of silicon nitride with $YAlO_3$ additive, J. Am. Ceram. Soc. 76 (9) (1993) 2373–2375.
[16] Y. Goto, G. Thomas, Phase transformation and microstructural changes of Si_3N_4 during sintering, J. Mater. Sci. 30 (1995) 2194–2200.
[17] A.G. Evans, E.A. Charles, Fracture toughness determinations by indentation, J. Am. Ceram. Soc. 59 (7/8) (1976) 371–391.
[18] L.J. Gauckler, H. Hohnke, T.Y. Tien, The system Si_3N_4–SiO_2–Y_2O_3, J. Ceram. Soc. 63 (1/2) (1980) 35–37.
[19] U. Kolitsch, H.J. Seifert, T. Ludwig, F. Aldinger, Phase equilibria and crystal chemistry in the Y_2O_3–Al_2O_3–SiO_2 system, J. Mater. Res. 14 (2) (1999) 447–455.
[20] T. Kawashima, H. Okamoto, H. Yamamoto, A. Kitamura, Gain size dependence of the fracture toughness of silicon nitride ceramics, J. Ceram. Soc. Jpn. 99 (4) (1999) 320–323.
[21] S. Mitomo, M. Uenosono, Microstructural development during gas-pressure sintering of α-silicon nitride, J. Am. Ceram. Soc. 75 (1) (1992) 103–108.
[22] M. Mitomo, In-situ microstructural control in engineering ceramics, Key Eng. Mater. 161–163 (1999) 53–58.
[23] K.H. Jack, Sialons: a study in materials development, in: S. Hampshire (Ed.), Non-oxide Technical and Engineering Ceramics, Elsevier Applied Science, London, 1986, pp. 1–29.
[24] K. Yabuta, H. Nishio, K. Uematsu, Effect of phase composition on the mechanical properties of hot pressed SiAlON ceramics, J. Am. Ceram. Soc. 74 (4) (1991) 884–886.
[25] K. Yabuta, H. Nishio, Effect of heating rate on transition liquid-phase sintering of β′-O′ sialon ceramics, J. Ceram. Soc. Jpn. 103 (1995) 1302–1304.